A general class of non-linear kinematic models to predict mean stress relaxation and multiaxial ratcheting in fatigue problems – Part II: Generalized surface translation rule ☆

Marco Antonio Meggiolaro [a,*], Jaime Tupiassú Pinho de Castro [a], Hao Wu [b], Eleazar Cristian Mejia Sanchez [a]

[a] *Department of Mechanical Engineering, Pontifical Catholic University of Rio de Janeiro, Rua Marquês de São Vicente 225 – Gávea, Rio de Janeiro, RJ 22451-900, Brazil*
[b] *School of Aerospace Engineering and Applied Mechanics, Tongji University, 1239 Siping Road, Shanghai, PR China*

ABSTRACT

Part I of this work introduced efficient reduced-order five-dimensional (5D) stress and strain spaces that can be used to predict ratcheting and mean stress relaxation phenomena at a much lower computation cost than in traditional 6D formulations. These 5D spaces were then applied to the qualitative study of uniaxial ratcheting, multiaxial ratcheting, and mean stress relaxation. Several non-linear kinematic (NLK) hardening models have been proposed to capture these effects in incremental plasticity simulations. In this Part II, an incremental plasticity formulation is proposed in the adopted 5D spaces, while its advantages over the classical 6D formulation are discussed. The 5D version of the main NLK models proposed in the literature are presented, which allows the definition of a unified generalized equation. The physical and geometrical interpretation of the hardening, dynamic recovery, and radial return terms from the proposed generalized equation are presented. Several surface translation rules can be represented as a particular case of the proposed model, including the ones by Chaboche (1979), Burlet–Cailletaud (1986), Ohno–Wang (1993), Jiang–Sehitoglu (1996), Bari–Hassan (2001) and Chen–Jiao (2004), among others. The adopted hardening surface representation can be used not only for the studied NLK models, but also to reproduce the Mróz–Garud multi-surface approach. Uniaxial ratcheting, multiaxial ratcheting, and mean stress relaxation experiments with 316L and 1020 steel tubular and cylindrical specimens are conducted to validate the proposed models.

© 2015 Elsevier Ltd. All rights reserved.

1. Introduction

The Bauschinger effect, observed under cyclic loading and commonly called *kinematic hardening*, is a change in the absolute value of the opposite yield strength after strain hardening, due to the microscopic stress distribution. Fig. 1 exemplifies the Bauschinger effect for a uniaxial load history represented in the $\sigma_x \times \tau_{xy}\sqrt{3}$ von Mises diagram. In this example, the von Mises yield surface $\sigma_{Mises} = S_Y$, which is the equation that describes the combinations of stress components that cause yielding, is allowed to translate with no change in its shape or radius $S = S_Y$. If the center of the yield surface is translated in the x direction of the von Mises stress space

by $(\sigma_{max} - S_Y)$, then the resulting surface will intersect the x axis in the new tensile yield stress $(\sigma_{max} - S_Y + S_Y) = \sigma_{max}$ and in the new compressive yield stress $(\sigma_{max} - S_Y - S_Y) = (\sigma_{max} - 2S_Y)$.

The new center of the yield surface is commonly called *backstress*, represented here by the stress vector $\vec{\beta}$, which is responsible for storing the plastic memory. In this 2D example, the tensile yielding from the first cycle would change the backstress in the $\sigma_x \times \tau_{xy}\sqrt{3}$ diagram from its initial value $\vec{\beta} \equiv \begin{bmatrix} \beta_x & \beta_y \end{bmatrix}^T = \begin{bmatrix} 0 & 0 \end{bmatrix}^T$ to $\vec{\beta} \equiv \begin{bmatrix} \beta_x & \beta_y \end{bmatrix}^T = \begin{bmatrix} \sigma_{max} - S_Y & 0 \end{bmatrix}^T$, see Fig. 1.

For a general multiaxial stress state, a 6D (instead of 2D) yield surface equation $Y = 0$ is adopted, usually based on the von Mises criterion if the material is isotropic. The von Mises yield surface can be represented as a hyper-sphere with radius $S \cdot \sqrt{2/3}$ in Voigt–Mandel's 6D deviatoric space, since

$$\vec{s} = \begin{bmatrix} s_x & s_y & s_z & \tau_{xy}\sqrt{2} & \tau_{xz}\sqrt{2} & \tau_{yz}\sqrt{2} \end{bmatrix}^T$$
$$\Rightarrow Y = (3/2) \cdot \left[|\vec{s}|^2 - (S \cdot \sqrt{2/3})^2 \right] = 0 \tag{1}$$
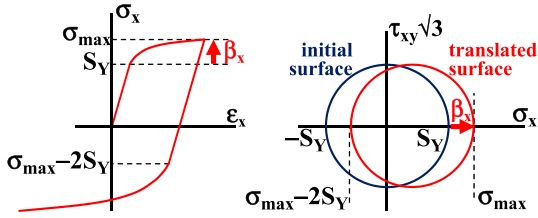
Fig. 1. Kinematic hardening in the x direction and associated Mises yield surface translation in the $\sigma_x \times \tau_{xy}\sqrt{3}$ diagram.

But a more convenient and computationally-efficient representation uses the E_{5s} stress space defined in Part I of this work, where the yield surface becomes a 5D hyper-sphere with radius S, since $|\vec{s}'| = S$, with the 5D deviatoric stress vector defined as

$$\vec{s}' \equiv \begin{bmatrix} s_1 & s_2 & s_3 & s_4 & s_5 \end{bmatrix}^T$$
$$= \begin{bmatrix} \sigma_x - \frac{\sigma_y + \sigma_z}{2} & \frac{\sigma_y - \sigma_z}{2}\sqrt{3} & \tau_{xy}\sqrt{3} & \tau_{xz}\sqrt{3} & \tau_{yz}\sqrt{3} \end{bmatrix}^T \qquad (2)$$

It was shown in Part I that the 6D and 5D spaces are related by a 5×6 transformation matrix A through

$$\vec{s}' = A \cdot \vec{\sigma} = A \cdot \vec{s}, \quad \vec{e}'_{el} = A \cdot \vec{\mathcal{E}}_{el} = A \cdot \vec{e}_{el}, \quad \vec{e}'_{pl} = A \cdot \vec{\mathcal{E}}_{pl} = A \cdot \vec{e}_{pl} \qquad (3)$$

where $\vec{\mathcal{E}}$, $\vec{e}$, and $\vec{e}'$ are respectively the 6D strain, 6D deviatoric strain, and 5D deviatoric strain, while the el and pl subscripts stand for their elastic and plastic components, and $\vec{\sigma}$ is the 6D stress.

Hooke's law is essentially represented in the same way in both 6D and 5D deviatoric spaces, because the relations $\vec{s}' = A \cdot \vec{s}$ and $\vec{e}'_{el} = A \cdot \vec{e}_{el}$ imply that

$$\vec{e}_{el} = \vec{s}/2G \Rightarrow A \cdot \vec{e}_{el} = A \cdot \vec{s}/2G \Rightarrow \vec{e}'_{el} = \vec{s}'/2G \qquad (4)$$

hence the deviatoric stress $\vec{s}'$ and elastic strain $\vec{e}'_{el}$ vectors are parallel and related by the scalar constant $2G$, a simple and convenient relation that further justifies the use of 5D stress and strain spaces.

But note that 5D formulations are not new, they have been originally proposed by Ilyushin [1], having been used in several multiaxial problems to calculate e.g.: (i) yield surface equations and failure criteria; (ii) path-equivalent stresses and strains using convex enclosures [2] or the Moment Of Inertia method [2,3]; (iii) multiaxial rainflow in the Modified Wang–Brown method [4]; and (iv) non-proportional hardening, using a 5D plastic strain space defined by Tanaka [5]. Nevertheless, incremental plasticity models are usually presented in a 6D formulation, performing 5D projections only after the calculation of the multiaxial stress–strain behavior, to perform multiaxial rainflow or path-equivalent calculations; or using a mixed 6D–5D formulation to compute non-proportional hardening transients, where 6D plastic strain increments are transformed to a 5D space at every cycle to compute Tanaka's 5×5 polarization matrix [5].

On the other hand, in this work the entire incremental plasticity formulation is presented in the adopted 5D spaces, which is surprisingly almost identical to the 6D formulation, except for scaling factors such as the $\sqrt{2/3}$ from the yield surface equations. One of the main advantages of the proposed 5D spaces is that the entire incremental plasticity formulation can be easily reduced to 3D, 2D, or 1D from the removal of appropriate rows from the deviatoric stress and strain vectors, as it was shown in Part I. For instance, incremental plasticity calculations for a tension–torsion history could be performed in the 2D sub-spaces $\vec{s}_{2D} \equiv \begin{bmatrix} s_1 & s_3 \end{bmatrix}^T$ and $\vec{e}_{2D} \equiv \begin{bmatrix} e_1 & e_3 \end{bmatrix}^T$ defined in Part I. This dimensional reduction would decrease computational cost in more than 50%, especially if non-proportional hardening transients are modeled, adopting a 2×2 polarization matrix instead of Tanaka's original 5×5 version defined in [5].

Kinematic hardening can be modeled in the 5D formulation (or in its 3D, 2D, or 1D sub-spaces) by allowing the yield surface $|\vec{s}'| = S$ to translate its center from the origin of the E_{5s} space to a 5D back-stress position $\vec{\beta}'$, becoming represented by $|\vec{s}' - \vec{\beta}'| = S$, with no change in its radius S or shape. Such translation is associated with plastic straining, usually assumed from the normality rule in the direction of the unit normal to the yield surface, defined as $\vec{n}$ for the 6D and $\vec{n}'$ for the adopted 5D formulation, evaluated at the current stress point. The Prandtl–Reuss plastic flow rule assumes that the magnitude of the plastic strain increment $d\vec{\mathcal{E}}_{pl}$ (in 6D) or $d\vec{e}'_{pl}$ (in 5D) depends on the applied stress increment, being inversely proportional to the generalized plastic modulus P that defines the slope between stress and plastic strain increments. The Prandtl–Reuss rule is usually defined in tensor or 6D notation, but it is easy to show from the relations $\vec{n}' = A \cdot \vec{n} \cdot \sqrt{2/3}$, $\vec{n} = A^T \cdot \vec{n}' \cdot \sqrt{2/3}$, and $A \cdot A^T = 1.5 \cdot I_{5 \times 5}$ (where $I_{5 \times 5}$ is the 5×5 identity matrix) that it has an almost identical version in the proposed 5D spaces:

$$d\vec{\mathcal{E}}_{pl} = \frac{1}{P} \cdot (d\vec{\sigma}^T \cdot \vec{n}) \cdot \vec{n} = \frac{1}{P} \cdot (d\vec{s}^T \cdot \vec{n}) \cdot \vec{n} \Rightarrow d\vec{e}''_{pl}$$
$$= \frac{1}{P} \cdot (d\vec{s}'^T \cdot \vec{n}') \cdot \vec{n}' \qquad (5)$$

using the same P without the need for a scaling factor.

There are several models to calculate the current value of the generalized plastic modulus P as the yield surface translates, as well as the direction of such translation, to obtain the associated plastic strain increments. Most of these hardening models can be divided into three classes: multi-surface [6,7], two-surface [8,9], and non-linear [10] kinematic hardening models.

Multi-surface kinematic hardening models assume that P is piecewise constant, resulting in a multi-linear description of the stress–strain curve, i.e. the non-linear shape of the stress–strain relation is approximated by several linear segments. Non-linear kinematic hardening models, on the other hand, are more general since they adopt non-linear equations to describe the surface translation direction and the value of P, leading to a more precise non-linear description of the stress–strain curve. A third class of kinematic hardening models involves the so-called two-surface models, which use a rather simplified formulation that combines elements of both non-linear and multi-surface kinematic models.

Multi-surface models cannot predict any uniaxial ratcheting or mean stress relaxation caused by unbalanced loadings, because their unrealistic perfectly symmetric hysteresis loops always close. In addition, under several non-proportional loading conditions, these models predict multiaxial ratcheting with a constant rate that never decays, severely overestimating the ratcheting effect measured in practice [11]. As a result, multi-surface kinematic hardening models should only be confidently applied to balanced proportional loading histories.

To correctly predict the stress–strain history associated with unbalanced loadings, it is necessary to use non-linear kinematic (NLK) models. Their original formulation [12] was improved by Chaboche [13], who indirectly introduced some multi-surface elements into the NLK models, however in a better non-linear instead of the simplistic multi-linear formulation.

In the following sections, the main NLK hardening models applicable to the prediction of ratcheting and mean stress relaxation are reviewed. A general hardening equation is presented, from which all NLK models are a special case. This equation is presented in the reduced-order five-dimensional space E_{5s} detailed in Part I of this work, which significantly decreases the computational cost in incremental plasticity calculations.

2. Multi-surface and non-linear kinematic (NLK) hardening models

Even though multi-surface models will not be simulated in this work, due to their inability to properly predict ratcheting and mean stress relaxation, their framework is detailed as follows. That is because Chaboche's 1979 contribution [13] to the NLK models indirectly made them adopt essentially the same multi-surface formulation, as proven in [14], however associated with non-linear instead of multi-linear incremental rules. The multi-surface formulation is presented next, in the proposed stress space E_{5s}.

2.1. Multi-surface formulation in 5D

Multi-surface models describe the behavior of elastoplastic solids from a family of nested surfaces in the stress space [6], the innermost being the yield surface associated with a yield strength S. In this work, instead of defining the nested surfaces in the 6D stress or 6D deviatoric stress spaces, the 5D reduced-order deviatoric stress space E_{5s} defined in Part I is adopted, using the von Mises yield function to describe each surface. As mentioned before, this 5D space has several advantages over the 6D formulations, since it is a non-redundant representation of the deviatoric stresses, which decreases the computational cost of stress–strain calculations. Although all kinematic hardening equations are presented here in the 5D space, their conversion to and from their original 6D versions is trivial, as it will be shown later.

Fig. 2 shows the family of nested surfaces that store plastic memory, represented in a sub-space $s_1 \times s_2$ of the 5D space E_{5s}. The first and innermost circle in Fig. 2 is the yield surface (either monotonic or cyclic), with radius $r_1 \equiv S$ (without the need for the scaling factor $\sqrt{2/3}$). In addition, $M-1$ *hardening surfaces* with radii $r_1 < r_2 < \cdots < r_{M+1}$ are defined, along with an outermost *failure surface* whose radius r_{M+1} is equal to the true rupture stress σ_U of the material. Their centers are located at points $\vec{s}_{ci}$ with $i = 2, 3, \ldots, M+1$, respectively. These $M+1$ nested circles cannot cross each other, must have increasing radii, and for a virgin material be initially concentric at the origin of the E_{5s} space, i.e. initially their $\vec{s}_{ci} = 0$. Moreover, the failure surface never translates, i.e. its center is always at the origin of the E_{5s} space, $\vec{s}_{c_{M+1}} \equiv 0$. Indeed, any stress point that reaches its boundary causes the material to locally fracture due to ductility exhaustion, which is equivalent to the criterion $|\vec{s}'| = r_{M+1} = \sigma_U$.

However, all other hardening surfaces can translate while the material strain-hardens, as shown in the arbitrary arrangement in Fig. 2. The surface centers move as the material plastically deforms and hardens. The difference between the radii of each pair of consecutive surfaces in the proposed E_{5s} space is defined as $\Delta r_i \equiv r_{i+1} - r_i$. In principle, all radii r_i may change during plastic deformation as a result of isotropic and non-proportional hardening effects, which would require additional equations such as the Voce and Tanaka's rule [5].

The backstress vector $\vec{\beta}'$, which locates the current yield surface center $\vec{\beta}' \equiv \vec{s}'_{c_1}$, can be decomposed as the sum of up to M surface backstresses $\vec{\beta}'_1, \vec{\beta}'_2, \ldots, \vec{\beta}'_M$ that describe the relative positions $\vec{\beta}'_i = \vec{s}'_{c_i} - \vec{s}'_{c_{i+1}}$ between centers of consecutive surfaces, see Fig. 2 (which depicts a case with $M = 3$). Note that the length (norm) $|\vec{\beta}'_i|$ of each surface backstress in this 5D representation is always between $|\vec{\beta}'_i| = 0$, if the surface centers $\vec{s}'_{c_i}$ and $\vec{s}'_{c_{i+1}}$ coincide (as in the unhardened condition from Fig. 3), and $|\vec{\beta}'_i| = \Delta r_i$, if the surfaces are mutually tangent (a saturation condition with maximum hardening, see Fig. 3). In the saturated condition for surface i, the surface backstress $\vec{\beta}'_i$ is aligned with the normal vector $\vec{n}'$ that is perpendicular to these mutually tangent surfaces at the current deviatoric stress state $\vec{s}'$, see Fig. 3, resulting in $\vec{\beta}'_i = \vec{n}' \cdot (r_{i+1} - r_i) = \vec{n}' \cdot \Delta r_i$.

2.2. Multi-surface model drawbacks

The multi-surface models proposed by Mróz [6] and Garud [7] use the above formulation (either in the original 6D version or in the proposed 5D spaces), however they assume that each hardening surface has its own generalized plastic modulus P, therefore it is piecewise-constant, generating a multi-linear description of stress–strain curves. Such description usually provides good results for balanced proportional loadings, explaining their use in several multiaxial fatigue problems involving balanced loadings.

But such multi-linear models cannot predict any uniaxial ratcheting or mean stress relaxation caused by unbalanced proportional loadings. This shortcoming is due to the linearity of the multi-surface translation rules and the resulting multi-linearity of the stress–strain representation, which describes all hysteresis loops using multiple straight segments, instead of predicting the experimentally observed curved paths caused by non-linear effects. Such straight segments generate unrealistic perfectly symmetric hysteresis loops that always close under constant amplitude proportional loadings, unable to predict uniaxial ratcheting or mean stress relaxation.

In addition, for NP loadings, multi-surface models may predict multiaxial ratcheting with a constant rate that never decays, severely overestimating the ratcheting effect measured in practice. As a result, multi-surface kinematic hardening models should only be applied to balanced loading histories, severely limiting their application.

These major drawbacks are a consequence of multi-surface kinematic hardening models being of an "uncoupled formulation" type, as qualified in [15]. Such uncoupling means that the generalized plastic modulus P in the multi-surface formulation is not a function of the straining direction. Such "uncoupled procedure"

Fig. 2. Initial yield, hardening, and failure surfaces for $M = 3$ in the $s_1 \times s_2$ deviatoric stress sub-space of E_{5s}, showing the backstress vector $\vec{\beta}'$ that defines location of the yield surface center $\vec{s}'_{c_1}$ and its components $\vec{\beta}'_1, \vec{\beta}'_2$, and $\vec{\beta}'_3$ that describe the relative positions between the centers of consecutive surfaces.
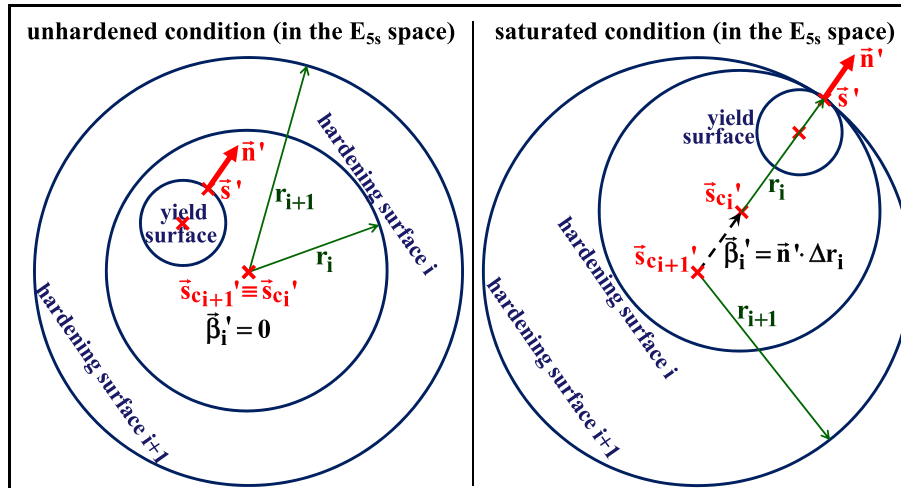
Fig. 3. Unhardened (left) and saturated (right) configurations of consecutive hardening surfaces i and $i + 1$ in the proposed E_{5s} stress space, respectively associated with $\vec{\beta}'_i = 0$ and $(\vec{\beta}'_i = \vec{n}' \cdot (r_{i+1} - r_i) = \vec{n}' \cdot \Delta r_i$.

provides undesirable additional degrees of freedom to the multi-surface models that allow, for instance, 90° out-of-phase tension–torsion predictions with resulting plastic strain amplitudes that are not a monotonic function of the applied stress amplitudes, as they should be [16]. These wrong multi-surface predictions are both qualitatively and quantitatively dependent on the number of surfaces adopted in the model, without any clear convergence.

To correctly predict the stress–strain history associated with unbalanced loadings, it is necessary to couple the values of the generalized plastic modulus P and the straining direction, in addition to introducing non-linearity in the surface translation equations, generating the non-linear kinematic (NLK) models. Note that the same multi-surface formulation presented in Section 2.1 can be used for NLK models, since the seminal work by Chaboche et al. [13], who indirectly introduced multi-surface elements into NLK models.

2.3. Multi-surface formulation in 5D for NLK hardening models

The first non-linear kinematic hardening model was proposed by Armstrong and Frederick in 1966 [12]. Their original single-surface model did not include any additional hardening surface, but their single yield surface already translated according to a non-linear rule. Since then, several improvements on Armstrong–Frederick's original NLK model have been proposed in the literature.

Fortunately, the exact same representation of the hardening state defined in Section 2.1 for multi-surface models, which includes one inner yield surface, $M - 1$ hardening surfaces, and one failure surface, can be used in the NLK hardening formulation, as it was demonstrated in [14]. Once again, instead of defining these surfaces in the 6D stress or deviatoric stress spaces, the proposed 5D reduced order deviatoric stress space E_{5s} is adopted, using the von Mises yield function to describe each surface. All kinematic hardening equations are presented in such 5D space, while their conversion to the 6D versions is trivial, as summarized in Table 1.

Similarly to multi-surface models, the backstress vector $\vec{\beta}'$ that locates the center of the yield surface can be decomposed as the sum of M surface backstresses $\vec{\beta}'_1, \vec{\beta}'_2, \ldots, \vec{\beta}'_M$ that describe the relative positions $\vec{\beta}'_i = \vec{s}_{c_i} - \vec{s}_{c_{i+1}}$ between the centers of consecutive yield surfaces, as proposed by Chaboche in 1979 [13], significantly improving the Armstrong–Frederick model capabilities by

indirectly introducing the concept of multiple hardening surfaces. Therefore, Figs. 2 and 3 and all their variables defined for the multi-surface models can also be used in the NLK formulation.

One of their main differences is that in multi-surface models each hardening surface would only translate if the stress point was located on its border, while in NLK models all yield and hardening surfaces translate during a plastic straining process (but with different rates). The initial yield and the additional hardening surfaces from the NLK hardening models behave as if they were all attached to one another with non-linear spring-slider elements, causing coupled translations even before they enter in contact. Therefore, any yield surface translation causes all hardening surfaces to translate, usually with different magnitudes and directions, even before they become tangent to each other. Such coupling among surfaces allows the NLK models to introduce the necessary non-linearity in the stress–strain description.

Pairs of consecutive yield surfaces i and $i + 1$ eventually become mutually tangent if $|\vec{\beta}'_i| = \Delta r_i$ (the 5D saturation condition), when their respective translations $d\vec{s}_{c_i}$ and $d\vec{s}_{c_{i+1}}$ will have the same magnitude and direction, therefore $d\vec{\beta}'_i = d\vec{s}_{c_i} - d\vec{s}_{c_{i+1}} = 0$, i.e. a zero surface backstress variation. In other words, in the proposed 5D formulation, plastic straining causes increments $d\vec{\beta}'_i \neq 0$ in all backstress components, except for the saturated surfaces, therefore during plastic straining

$$d\vec{\beta}'_i = \begin{cases} p_i \cdot \vec{v}'_i \cdot dp, & \text{if } |\vec{\beta}'| < \Delta r_i \\ 0, & \text{if } |\vec{\beta}'| = \Delta r_i \end{cases}, \quad i = 1, 2, \ldots, M \quad (6)$$

where $\vec{v}'_i$ is the translation direction vector for surface i, dp is the equivalent plastic strain increment, calculated in the proposed 5D E_{5p} plastic strain space as $dp = (2/3) \cdot |d\vec{e}'_{pl}|$, and p_i is a generalized plastic modulus coefficient that must be calibrated for every surface, used in the calculation of P.

The main difference among the several NLK hardening models proposed in the literature rests in the equation of the surface translation direction $\vec{v}'_i$. In the next section, a generalized surface translation rule is proposed in the adopted 5D E_{5s} stress space, which is able to unify all major NLK models into a single equation.

3. Generalized surface translation rule

The generalized surface translation rule proposed in this work can be written as

Table 1
Incremental plasticity equations using the proposed 5D or the classical 6D deviatoric formulations.

	Proposed 5D formulation	6D formulation
Vector norm	$\|\vec{s}'\| = \sigma_{Mises}$	$\|\vec{s}\| = \sigma_{Mises}\sqrt{2/3}$
Hooke's law	$\vec{e}'_{el} = \vec{s}'/2G, \ d\vec{e}'_{el} = d\vec{s}'/2G$	$\vec{e}_{el} = \vec{s}/2G, \ d\vec{e}_{el} = d\vec{s}/2G$
Plastic flow rule	$d\vec{e}'_{pl} = (1/P) \cdot (d\vec{s}'^T \cdot \vec{n}') \cdot \vec{n}'$	$d\vec{e}_{pl} = d\vec{e}_{pl} = (1/P) \cdot (d\vec{s}^T \cdot \vec{n}) \cdot \vec{n}$
Direct problem	$d\vec{e}' = (d\vec{s}'/2G) + (1/P) \cdot (d\vec{s}'^T \cdot \vec{n}') \cdot \vec{n}'$	$d\vec{e} = (d\vec{s}/2G) + (1/P) \cdot (d\vec{s}^T \cdot \vec{n}) \cdot \vec{n}$
	$d\vec{\varepsilon} = (2/3) \cdot A^T \cdot d\vec{e}' + d\vec{\sigma}_h/3\mathcal{K}$	$d\vec{\varepsilon} = d\vec{e} + d\vec{\varepsilon}_h/3\mathcal{K}$
Inverse problem	$d\vec{s}' = 2G \cdot \left[d\vec{e}' - \frac{2G \cdot (d\vec{e}'^T \cdot \vec{n}') \cdot \vec{n}'}{2G+P} \right]$	$d\vec{s} = 2G \cdot \left[d\vec{e} - \frac{2G \cdot (d\vec{e}^T \cdot \vec{n}) \cdot \vec{n}}{2G+P} \right]$
	$d\vec{\sigma} = 2A^T \cdot d\vec{s}'/3 + 3\mathcal{K} \cdot d\vec{\varepsilon}_h$	$d\sigma = d\vec{s} + 3\mathcal{K} \cdot d\vec{\varepsilon}_h$
Normal vector	$\vec{n}' = \frac{\vec{s}' - \vec{\beta}'}{\sigma_{Mises}} = A \cdot n \cdot \sqrt{2/3}$	$\vec{n} = \frac{\vec{s} - \vec{\beta}}{\sigma_{Mises}\sqrt{2/3}} = A^T \cdot \vec{n}' \cdot \sqrt{2/3}$
Consistency	$d\vec{s}'^T \cdot \vec{n}' = d\vec{\beta}'^T \cdot \vec{n}' + dS$	$d\vec{s}^T \cdot \vec{n} = d\vec{\beta}^T \cdot \vec{n} + dS \cdot \sqrt{2/3}$
Surface radii	r_i (with $\Delta r_i = r_{i+1} - r_i$)	$r_i^* = r_i\sqrt{2/3}$ (with $\Delta r_i^* = \Delta r_i\sqrt{2/3}$)
NLK hardening	$d\vec{\beta}'_i = \begin{cases} p_i \cdot \vec{v}'_i \cdot dp, & \text{if } \|\vec{\beta}'_i\| < \Delta r_i \\ 0, & \text{if } \|\vec{\beta}'_i\| = \Delta r_i \end{cases}$	$d\vec{\beta}_i = \begin{cases} p_i \cdot \vec{v}_i \cdot dp, & \text{if } \|\vec{\beta}_i\| < \Delta r_i^* \\ 0, & \text{if } \|\vec{\beta}_i\| < \Delta r_i^* \end{cases}$
	$\vec{v}'_i = \vec{n}' \cdot \Delta r_i - \chi_i^* \cdot m_i^* \cdot \gamma_i \cdot [\delta_i \cdot \vec{\beta}'_i + (1 - \delta_i) \cdot (\vec{\beta}'^T_i \cdot \vec{n}') \cdot \vec{n}']$	$\vec{v}_i = \vec{n} \cdot \Delta r_i^* - \chi_i^* \cdot m_i^* \cdot \gamma_i \cdot [\delta_i \cdot \vec{\beta}_i + (1 - \delta_i) \cdot (\vec{\beta}^T_i \cdot \vec{n}) \cdot \vec{n}]$
	$m_i^* \equiv \begin{cases} \left(\vec{\beta}'^T_i \cdot \vec{n}'/\|\vec{\beta}'_i\| \right)^{m_i}, & \text{if } \vec{\beta}'^T_i \cdot \vec{n}' \geqslant 0 \\ 0, & \text{if } \vec{\beta}'^T_i \cdot \vec{n}' < 0 \end{cases}$	$m_i^* \equiv \begin{cases} \left(\vec{\beta}^T_i \cdot \vec{n}/\|\vec{\beta}_i\| \right)^{m_i}, & \text{if } \vec{\beta}^T_i \cdot \vec{n} \geqslant 0 \\ 0, & \text{if } \vec{\beta}^T_i \cdot \vec{n} < 0 \end{cases}$
	$\chi_i^* \equiv (\|\vec{\beta}'_i\|/\Delta r_i)^{\chi_i}$	$\chi_i^* \equiv \left(\|\vec{\beta}_i\|/\Delta r_i^* \right)^{\chi_i}$
	$P = \sum_{i=1}^{M} \frac{2p_i(\Delta r_i - \chi_i^* \cdot m_i^* \cdot \gamma_i \cdot \vec{\beta}'^T_i \cdot \vec{n}')}{3}$	$P = \sqrt{\frac{2}{3}}\sum_{i=1}^{M} p_i \left(\Delta r_i^* - \chi_i^* \cdot m_i^* \cdot \gamma_i \cdot \vec{\beta}'^T_i \cdot \vec{n}' \right)$

$$\vec{v}'_i = \underbrace{\vec{n}' \cdot \Delta r_i}_{Prager-Ziegler} - \chi_i^* \cdot m_i^* \cdot \gamma_i$$
$$\cdot \left[\underbrace{\delta_i \cdot \vec{\beta}'_i}_{\text{dynamic recovery}} + \underbrace{(1 - \delta_i) \cdot (\vec{\beta}'^T_i \cdot \vec{n}') \cdot \vec{n}'}_{\text{radial return}} \right] \quad (7)$$

where the scalar functions χ_i^* and m_i^* are defined as

$$\chi_i^* \equiv \left(\frac{\|\vec{\beta}'_i\|}{\Delta r_i} \right)^{\chi_i} \quad \text{and} \quad m_i^* \equiv \begin{cases} \left[\vec{\beta}'^T_i \cdot \vec{n}'/\|\vec{\beta}'_i\| \right]^{m_i}, & \text{if } \vec{\beta}'^T_i \cdot \vec{n}' \geqslant 0 \\ 0, & \text{if } \vec{\beta}'^T_i \cdot \vec{n}' < 0 \end{cases} \quad (8)$$

This function is a further generalization of the (already general) class of hardening rules defined in [17], which only included the Prager–Ziegler and dynamic recovery terms from Eq. (7), but not the radial return term (discussed later on), i.e. it always assumed that $\delta_i = 1$.

The calibration parameters for each hardening surface i are the ratcheting exponent χ_i, the multiaxial ratcheting exponent m_i, the ratcheting coefficient γ_i, and the multiaxial ratcheting coefficient δ_i,

which are scalar values listed in Table 2 for several popular models. Note that several references represent the NLK hardening parameters Δr_i, p_i and χ_i using respectively the terms $r^{(i)}$, $c^{(i)}$ and $\chi^{(i)}$, however this notation is not used in this work to avoid mistaking the (i) superscripts for exponents, as well as to emphasize the geometrical meaning of the Δr_i parameters, which are differences between radii of consecutive surfaces.

The 5D translation direction $\vec{v}'_i$ of each surface from Eq. (7) can be separated into three components: (i) the Prager–Ziegler term, in the normal direction $\vec{n}'$ perpendicular to the yield surface; (ii) the dynamic recovery term, in the opposite direction $-\vec{\beta}'_i$ of the back-stress of the considered surface, which acts as a recall term that gradually erases plastic memory with an intensity proportional to the product $\chi_i^* \cdot m_i^* \cdot \gamma_i \cdot \delta_i$; and (iii) the radial return term, in the opposite direction $-\vec{n}'$ of the normal vector, which affects multiaxial ratcheting predictions, calibrated from $\chi_i^* \cdot m_i^* \cdot \gamma_i \cdot (1 - \delta_i) \cdot \left(\vec{\beta}'^T_i \cdot \vec{n}' \right)$.

Fig. 4 shows the geometric interpretation of these three components. The dynamic recovery term deviates the surface translation

Table 2
Calibration parameters for the general translation direction from Eqs. (7) and (8).

Year	Kinematic model	χ_i	m_i	γ_i	δ_i
1949	Prager [18]	0	0	0	1
1966	Armstrong–Frederick [12]	0	0	$0 \leqslant \gamma_i \leqslant 1$	1
1967	Mróz [6]	0	0	1	1
1979	Chaboche [13]	1	0	1	1
1986	Burlet–Cailletaud [20]	0	0	$0 \leqslant \gamma_i \leqslant 1$	0
1993	Ohno–Wang I [21–22]	∞	1	1	1
1993	Ohno–Wang II [21–22]	$0 \leqslant \chi_i < \infty$	1	1	1
1995	Delobelle [24]	0	0	$0 \leqslant \gamma_i \leqslant 1$	$0 \leqslant \delta_i \leqslant 1$
1996	Jiang–Sehitoglu [17,23]	$0 \leqslant \chi_i < \infty$	0	1	1
2004	Chen–Jiao [26]	$0 \leqslant \chi_i < \infty$	1	1	$0 \leqslant \delta_i \leqslant 1$
2005	Chen–Jiao–Kim [25]	$0 \leqslant \chi_i < \infty$	$-\infty < m_i < \infty$	1	1
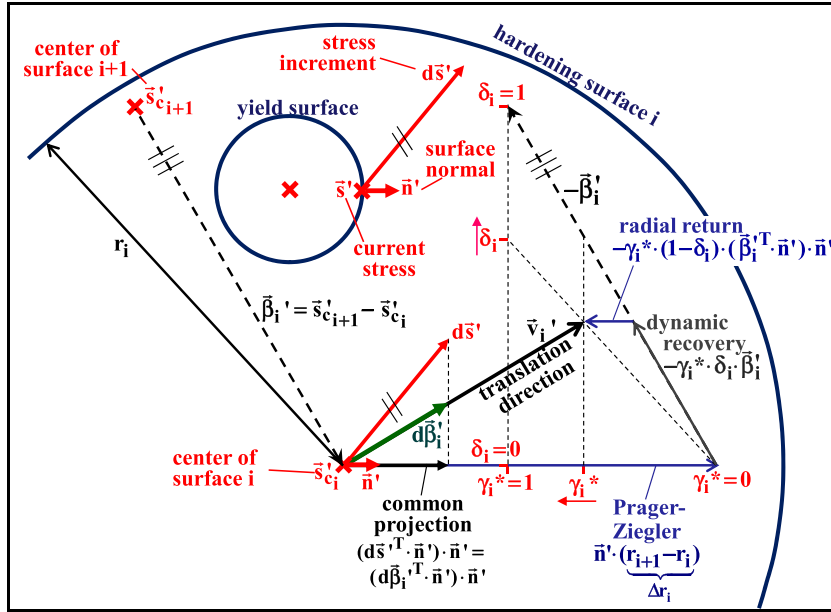
Fig. 4. Geometric interpretation of the three components of the translation direction $\vec{v}_i'$ of a hardening surface i, in the proposed E_{5s} stress space: Prager–Ziegler's, dynamic recovery, and radial return terms, where the equivalent parameter $\gamma_i \equiv \chi_i^* \cdot m_i^* \cdot \gamma_i$.

direction $\vec{v}_i'$ from the normal direction $\vec{n}'$, while the radial return term reduces the magnitude of the normal component from its original Prager–Ziegler term $\vec{n}' \cdot \Delta r_i$. Both dynamic recovery and radial return terms from each surface i are influenced by all four calibration parameters χ_i, m_i, γ_i and δ_i, which are further explained as follows.

Among the models included in Table 2, Prager's [18] translation direction $\vec{v}_i' = \vec{n}' \cdot \Delta r_i$ is not able to predict uniaxial ratcheting since it only uses the Prager–Ziegler term, which is linear. For multiaxial ratcheting, it only predicts a very short transient that almost immediately arrests (shakedown), highly underestimating multiaxial ratcheting rates. The translation direction $\vec{v}_i' = \vec{n}' \cdot \Delta r_i - \vec{\beta}_i'$ from Mróz [6] includes a dynamic recovery term, however in a linear formulation that highly overestimates multiaxial ratcheting. As discussed before, the Mróz rule cannot predict any uniaxial ratcheting at all when used in a multi-surface formulation, where the outer surfaces not touched by the current stress point are not allowed to translate. But when applied to the NLK formulation, where *all* surfaces translate during plastic straining, the Mróz translation direction becomes capable of predicting uniaxial ratcheting, albeit largely overestimating it.

Armstrong and Frederick proposed the use of a ratcheting coefficient $0 \leqslant \gamma_i \leqslant 1$, originally intended to be a scalar function of the plastic strain path, adding non-linearity to their hardening model [12]. This parameter has been included in the proposed 5D general surface translation rule. However, in many practical implementations, γ_i was assumed as a constant, turning their translation equation $\vec{v}_i' = \vec{n}' \cdot \Delta r_i - \gamma_i \cdot \vec{\beta}_i'$ into a linear rule that suffers the same drawbacks of the Mróz translation rule in the NLK formulation, with a large overestimation of both uniaxial and multiaxial ratcheting. Even though γ_i can calibrate ratcheting rates, with the limit values $\gamma_i = 0$ (Prager's rule) for no ratcheting and $\gamma_i = 1$ (Mróz rule) for large ratcheting rates, the linearity associated with a constant γ_i makes it impossible to predict multiaxial ratcheting rate decay and arrest (shakedown) observed in several constant amplitude experiments. In addition, for constant coefficients $\gamma_i < 1$, the Armstrong–Frederick translation rule would result in $d\vec{\beta}_i' \neq 0$ in the saturated condition, which would allow the surfaces to pass through one another. To avoid this, it has been proposed to simply enforce

$\gamma_i = 1$ in the saturation condition $|\vec{\beta}_i'| = \Delta r_i$, while allowing the use of a calibrated $\gamma_i < 1$ for $|\vec{\beta}_i'| < \Delta r_i$ [19]. Both Armstrong–Frederick and Mróz rules are a particular case of the proposed generalized surface translation rule from Eqs. (7) and (8), for $\chi_i = m_i = 0$, $\delta_i = 1$, and an adjustable $0 \leqslant \gamma_i \leqslant 1$ that for Mróz is set to $\gamma_i = 1$.

Chaboche [13] replaced the constant ratcheting coefficient γ_i with a saturation ratio, which in the proposed 5D formulation is represented as $|\vec{\beta}_i'|/\Delta r_i$, ranging from 0 in the unhardened condition to 1 at saturation, eliminating the discontinuity problem caused by $\gamma_i \neq 1$. But even though the resulting surface translation rule (represented in its 5D version)

$$\vec{v}_i' = \vec{n}' \cdot \Delta r_i - \left(|\vec{\beta}_i'|/\Delta r_i \right) \cdot \vec{\beta}_i' \quad \text{(5D Chaboche)} \tag{9}$$

is an improvement over the constant γ_i models such as Mróz and most implementations of Armstrong–Frederick, it is unable to predict multiaxial ratcheting rate decay and arrest. This model predicts a short ratcheting transient followed by a constant ratcheting rate that never decays, overestimating its effects in multiaxial experiments. Chaboche's model is also a particular case of Eqs. (7) and (8), for $\chi_i = 1$, $m_i = 0$, and $\gamma_i = \delta_i = 1$.

Burlet and Cailletaud noticed that multiaxial experiments generally show lower ratcheting rates than the uniaxial ones for equivalent conditions on stress or strain amplitudes [20]. To lower the multiaxial ratcheting rate predictions without altering the uniaxial response, they replaced the dynamic recovery term with a radial return term. In the 5D formulation adopted in this work, their surface translation direction becomes

$$\vec{v}_i' = \vec{n}' \cdot \Delta r_i - \gamma_i \cdot \left(\vec{\beta}_i'^T \cdot \vec{n}' \right) \cdot \vec{n}' \quad \text{(5D Burlet–Cailletaud)} \tag{10}$$

Burlet–Cailletaud's model is also obtained from the proposed Eqs. (7) and (8), assuming $\chi_i = m_i = \delta_i = 0$ and an adjustable $0 \leqslant \gamma_i \leqslant 1$.

The product $\vec{\beta}_i'^T \cdot \vec{n}'$ used in the radial return term measures the non-coaxiality between the surface backstress $\vec{\beta}_i'$ and the plastic strain increment direction $\vec{n}'$. As a result, it is a measure of non-proportionality, since parallel $\vec{\beta}_i'$ and $\vec{n}'$ usually found in proportional loadings result in $\vec{\beta}_i'^T \cdot \vec{n}' = \pm|\vec{\beta}_i'|$, while 90° out-of-phase loadings where plastic straining happens in a direction $\vec{n}'$

perpendicular to the surface backstress $\vec{\beta}_i'$ gives $\vec{\beta}_i'^T \cdot \vec{n}' = 0$. Such different products allow the model to predict non-proportional effects in multiaxial ratcheting.

In addition, the Burlet–Cailletaud's radial return term becomes identical to the Armstrong–Frederick's dynamic recovery term for uniaxial loadings, where parallel $\vec{\beta}_i'$ and $\vec{n}'$ make $\gamma_i \cdot (\vec{\beta}_i'^T \cdot \vec{n}') \cdot \vec{n}' = \gamma_i \cdot \vec{\beta}_i'$; therefore, both models behave identically under uniaxial conditions, overpredicting uniaxial ratcheting rates. Note that Burlet–Cailletaud's surface translation direction $\vec{v}_i'$ is always parallel to $\vec{n}'$, therefore it behaves similarly to Prager's rule under multiaxial loading conditions, largely underpredicting multiaxial ratcheting rates, which always rapidly decay in the simulations causing premature shakedown.

Ohno and Wang used the non-proportionality product (calculated in our 5D formulation from $\vec{\beta}_i'^T \cdot \vec{n}'$) in a different way [21,22]. For plastic straining in a direction $\vec{n}'$ that makes an obtuse angle with $\vec{\beta}_i'$, i.e. when $\vec{\beta}_i'^T \cdot \vec{n}' < 0$ (usually during an elastoplastic unloading process), they assumed that the translation direction follows Prager's linear rule $\vec{v}_i' = \vec{n}' \cdot \Delta r_i$. Otherwise, when $\vec{\beta}_i'^T \cdot \vec{n}' \geqslant 0$ (usually during an elastoplastic loading process), they introduced in their model a scalar function (given by $0 \leqslant \chi_i^* \equiv (|\vec{\beta}_i'|/\Delta r_i)^{\chi_i} \leqslant 1$ in the proposed 5D formulation) and a non-proportionality term (defined in 5D as $0 \leqslant (\vec{\beta}_i'^T \cdot \vec{n}'/|\vec{\beta}_i'|) \leqslant 1$), resulting in the "Ohno–Wang II" (OW-II) surface translation direction, whose 5D version in the E_{5s} stress space becomes

$$\vec{v}_i' = \vec{n}' \cdot \Delta r_i - \left(|\vec{\beta}_i'|/\Delta r_i \right)^{\chi_i} \cdot (\vec{\beta}_i'^T \cdot \vec{n}'/|\vec{\beta}_i'|) \cdot \vec{\beta}_i' \quad \text{(5D Ohno–Wang II)} \tag{11}$$

where χ_i ($0 \leqslant \chi_i \leqslant \infty$) is the ratcheting exponent. Surfaces calibrated with a very large χ_i (such as in their "Ohno–Wang I" OW-I model version that assumes $\chi_i \to \infty$) have $\chi_i^* \equiv 0$, which results in Prager's linear rule $\vec{v}_i' = \vec{n}' \cdot \Delta r_i$ for most of the range $0 \leqslant |\vec{\beta}_i'|/\Delta r_i \leqslant 1$ before saturation, becoming unable to predict uniaxial ratcheting. The dynamic recovery term would only be activated when the surfaces are closer to contacting each other, i.e. when $|\vec{\beta}_i'|/\Delta r_i \cong 1$. Lower calibrated values of χ_i, on the other hand, allow the dynamic recovery term to be partially operative in the entire $|\vec{\beta}_i'|/\Delta r_i$ range, increasing the predicted uniaxial ratcheting rates. So, in summary, lower calibrated values of χ_i result in higher uniaxial ratcheting rate predictions. Note that both OW-I and OW-II Ohno–Wang models are a particular case of the proposed Eqs. (7) and (8), adopting $m_i = \gamma_i = \delta_i = 1$, and an adjustable $0 \leqslant \chi_i < \infty$ that tends to infinity for the OW-I.

However, the ratcheting parameter χ_i influences both uniaxial and multiaxial ratcheting predictions. When χ_i is calibrated to fit uniaxial ratcheting data, the OW-II model ends up overestimating multiaxial ratcheting. In addition, although the OW-II model is able to predict multiaxial ratcheting rate decay, the use of a single calibration parameter χ_i renders it unable to model experiments with constant multiaxial ratcheting rates.

Jiang and Sehitoglu [17,23] improved the OW-II model to solve this last problem by simply removing the non-proportionality term ($\vec{\beta}_i'^T \cdot \vec{n}'/|\vec{\beta}_i'|$ in our 5D formulation) from its translation rule. When represented in the proposed E_{5s} stress space, Jiang–Sehitoglu's surface translation direction is expressed as

$$\vec{v}_i' = \vec{n}' \cdot \Delta r_i - \left(|\vec{\beta}_i'|/\Delta r_i \right)^{\chi_i} \cdot \vec{\beta}_i' \quad \text{(5D Jiang–Sehitoglu)} \tag{12}$$

where $0 \leqslant \chi_i < \infty$. This equation is used even during an elastoplastic unloading $\vec{\beta}_i'^T \cdot \vec{n}' < 0$, instead of switching to Prager's linear rule as it had been done by Ohno and Wang.

Jiang–Sehitoglu's equation is also a particular case of Eqs. (7) and (8), for $m_i = 0$ and $\gamma_i = \delta_i = 1$, similar to Chaboche's model [13], and with an adjustable $0 \leqslant \chi_i < \infty$. As a result, Jiang–Sehitoglu's equation is a generalized version of Chaboche's original model [13], which would be obtained for the particular case $\chi_i = 1$. Since Chaboche's model has the ability to predict constant ratcheting rate for both uniaxial and multiaxial loadings, Jiang–Sehitoglu's equation overcomes the inability of the OW-II model to predict constant multiaxial ratcheting rates. Multiaxial ratcheting rate decay can also be predicted, if a ratcheting rate exponent $\chi_i \neq 1$ is chosen in the calibration. Nevertheless, Jiang–Sehitoglu's model still relies on a single calibration parameter χ_i to predict both uniaxial and multiaxial ratcheting rates.

Calibrating a kinematic hardening model using different parameters to independently control uniaxial and multiaxial ratcheting allows for a much better description of the material behavior. This separation is necessary because both ratcheting types are caused by different phenomena: uniaxial ratcheting is a consequence of anisotropy between the tension and compression behaviors, as discussed in Part I of this work, while multiaxial ratcheting is associated with elastoplastic deviatoric stress increments $d\vec{s}'$ that are not parallel to the normal $\vec{n}'$ to the yield surface at the current state, causing plastic strains not only in the direction of $d\vec{s}'$ but also ratcheting strains in perpendicular directions. For instance, a material with a significant strength difference between tension and compression could have almost the same multiaxial ratcheting behavior as a perfectly isotropic one, even though only the former could suffer uniaxial ratcheting. It would be impossible to accurately calibrate both independent behaviors with a single scalar parameter for each surface such as χ_i.

Since Armstrong–Frederick's model largely underpredicts while Burlet–Cailletaud's largely overestimates multiaxial ratcheting rates, Delobelle et al. [24] decided to interpolate them using a multiaxial ratcheting coefficient δ_i ($0 \leqslant \delta_i \leqslant 1$). In the proposed E_{5s} space, Delobelle's surface translation direction becomes

$$\vec{v}_i' = \vec{n}' \cdot \Delta r_i - \gamma_i$$
$$\cdot \left[\delta_i \cdot \vec{\beta}_i' + (1 - \delta_i) \cdot (\vec{\beta}_i'^T \cdot \vec{n}') \cdot \vec{n}' \right] \quad \text{(5D Delobelle)} \tag{13}$$

The limit value $\delta_i = 0$ gives exactly the Burlet–Cailletaud model, associated with a large radial return term and zero dynamic recovery, a "radial evanescence" condition that results in low multiaxial ratcheting rates with large rate decay. The other limit value $\delta_i = 1$ gives exactly the Armstrong–Frederick model, with a large dynamic recovery term and zero radial return, the usual "backstress evanescence" condition that results in overestimated multiaxial ratcheting without rate decay, as discussed before. If $0 < \delta_i < 1$, then the predictions are somewhere in between the two limit cases, with δ_i acting as a weighting factor to calibrate the multiaxial ratcheting rates. The value of γ_i influences both uniaxial and multiaxial ratcheting estimations. However, the uniaxial ratcheting response is not affected by δ_i because, for uniaxial loadings, $\vec{\beta}_i'$ and $\vec{n}'$ are always parallel to the uniaxial direction, therefore the relation $\gamma_i \cdot (\vec{\beta}_i'^T \cdot \vec{n}') \cdot \vec{n}' = \gamma_i \cdot \vec{\beta}_i'$ causes a translation direction

$$\vec{v}_i' = \vec{n}' \cdot \Delta r_i - \gamma_i \cdot [\delta_i + (1 - \delta_i)] \cdot \vec{\beta}_i'$$
$$= \vec{n}' \cdot \Delta r_i - \gamma_i \cdot \vec{\beta}_i' \quad \text{(5D Delobelle — uniaxial case)} \tag{14}$$

that is independent of δ_i. So, γ_i must be calibrated first for every surface to fit uniaxial ratcheting data, and after that the δ_i values can be freely calibrated to multiaxial ratcheting data without affecting the previous uniaxial calibration. Delobelle's model is obtained from the generalized surface translation rule from Eqs. (7) and (8) for $\chi_i = m_i = 0$, and adjustable $0 \leqslant \gamma_i \leqslant 1$ and $0 \leqslant \delta_i \leqslant 1$ to

independently calibrate uniaxial and multiaxial ratcheting. Note however that, similarly to both Armstrong–Frederick and Burlet–Cailletaud equations, the Delobelle model still overpredicts uniaxial ratcheting rates, since the ratcheting coefficient γ_i is not as efficient as the ratcheting exponent χ_i to model uniaxial ratcheting rate decay or even growth as a function of the stress amplitude.

On the other hand, the Chen–Jiao–Kim model [25], in addition to the use of the better parameter χ_i to calibrate uniaxial ratcheting, is able to independently calibrate uniaxial and multiaxial ratcheting behaviors by incorporating a multiaxial ratcheting exponent m_i in the non-proportionality term $\vec{\beta}_i'^T \cdot \vec{n}'/|\vec{\beta}_i'|$ from the OW-II model. Therefore, for a multiaxial elastoplastic loading process with $\vec{\beta}_i'^T \cdot \vec{n}' \geqslant 0$, the scalar function $m_i^* \equiv (\vec{\beta}_i'^T \cdot \vec{n}'/|\vec{\beta}_i'|)^{m_i}$ is used to multiply the dynamic recovery term. In the proposed 5D formulation, Chen–Jiao–Kim's surface translation direction becomes

$$\vec{v}_i' = \vec{n}' \cdot \Delta r_i - (|\vec{\beta}_i'|/\Delta r_i)^{\chi_i} \cdot (\vec{\beta}_i'^T \cdot \vec{n}'/|\vec{\beta}_i'|)^{m_i} \cdot \vec{\beta}_i' \quad \text{(5D Chen—Jiao—Kim)} \tag{15}$$

where $0 \leqslant \chi_i < \infty$ and $-\infty < m_i < \infty$. For an elastoplastic unloading process with $\vec{\beta}_i'^T \cdot \vec{n}' < 0$, Prager's linear rule $\vec{v}_i' = \vec{n}' \cdot \Delta r_i$ is used instead. For uniaxial load histories during elastoplastic loading, where the relation $\vec{\beta}_i'^T \cdot \vec{n}' = |\vec{\beta}_i'|$ is always valid, the scalar function m_i^* simply becomes $m_i^* = (1)^{m_i} = 1$, therefore uniaxial ratcheting predictions are not affected by the calibrated value of m_i. Thus, χ_i should be calibrated first for the yield and every hardening surface to fit uniaxial ratcheting rate data, and after that the m_i values could be freely calibrated to correctly describe measured multiaxial ratcheting rates and decays without affecting the previous uniaxial calibration. Chen–Jiao–Kim's model can also be obtained from the general Eqs. (7) and (8) proposed in this work, adopting $\gamma_i = \delta_i = 1$, and independently adjustable $0 \leqslant \chi_i < \infty$ and $-\infty \leqslant m_i \leqslant \infty$.

A different approach for obtaining a simultaneous correct description of uniaxial and multiaxial ratcheting was adopted in the Chen–Jiao model [26]. This model uses Delobelle's [24] multiaxial ratcheting coefficient δ_i ($0 \leqslant \delta_i \leqslant 1$) instead of the multiaxial ratcheting exponent m_i, incorporated into Jiang–Sehitoglu's model to give, in the adopted E_{5s} space version,

$$\vec{v}_i' = \vec{n}' \cdot \Delta r_i - (|\vec{\beta}_i'|/\Delta r_i)^{\chi_i} \cdot [\delta_i \cdot \vec{\beta}_i' + (1 - \delta_i) \cdot (\vec{\beta}_i'^T \cdot \vec{n}') \cdot \vec{n}'] \quad \text{(5D Chen—Jiao)} \tag{16}$$

As in Delobelle's model, δ_i can calibrate multiaxial ratcheting data without affecting uniaxial ratcheting calculations. The exponent χ_i ($0 \leqslant \chi_i < \infty$) of the yield or every hardening surface should be calibrated first to accurately match uniaxial ratcheting data, and only then the δ_i should be fitted to describe multiaxial ratcheting rates

and decay. Chen and Jiao also refined the multiaxial ratcheting description, allowing the δ_i parameter from each surface to vary between an initial value and a target value δ_{ti}, with an evolution equation $d\delta_i = (\delta_{ti} - \delta_i) \cdot b_{CJ} \cdot dp$ controlled by the equivalent plastic strain increments dp, where b_{CJ} is the Chen–Jiao evolution rate. Note however that this refinement introduces the additional parameters δ_{ti} (one for each surface i) and b_{CJ}, which would need to be calibrated in proper tests. Finally, note that Chen–Jiao's model is also a particular case of the proposed Eqs. (7) and (8), adopting $m_i = \gamma_i = 1$, and independently adjustable $0 \leqslant \chi_i < \infty$ and $0 \leqslant \delta_i \leqslant 1$.

Table 2 summarizes the calibration parameter choices for the general translation direction from Eqs. (7) and (8), showing that all presented models are a particular case of the proposed expression. Table 3 summarizes the advantages and disadvantages of the various equations that intend to describe the yield surface translation direction $\vec{v}_i'$. Note that independent calibration of uniaxial and multiaxial ratcheting rates can only be achieved using equations with at least two parameters per surface (i.e. a total of at least $2M$ parameters for M yield and hardening surfaces), such as the Delobelle, Chen–Jiao, and Chen–Jiao–Kim equations. However, Delobelle's model still overpredicts uniaxial ratcheting rates, due to the use of the ratcheting coefficient γ_i instead of the better ratcheting exponent χ_i to calibrate them. Nevertheless, if the studied load history only causes significant uniaxial or multiaxial ratcheting, but not both, then Jiang–Sehitoglu's equation would also be a good modeling choice, since it can calibrate arbitrary uniaxial or multiaxial ratcheting rates, including multiaxial ratcheting with constant rate or rate decay, using only the M ratcheting exponents χ_i from the M surfaces, without requiring the (possibly less robust) calibration of $2M$ or more parameters.

The fitting of the generalized plastic modulus coefficients p_i from each surface for a given Δr_i, see Eq. (6), as well as the calibration of the ratcheting coefficients χ_i, m_i, γ_i, and/or δ_i, depend on the adopted NLK model. Approximate fitting algorithms for the parameter pairs (p_i, χ_i) or $(\Delta r_i, \chi_i)$ are shown in [23] for Jiang–Sehitoglu's model, which can be easily adapted from the 6D to the proposed 5D formulation, however they are precise only for materials with very large ratcheting exponents χ_i. For other cases, a least-squares fitting approach should be adopted to calibrate such parameters, comparing experimental measurements with incremental plasticity simulations.

4. Consistency condition formulation in 5D

Any straining process within the yield surface is assumed purely elastic, so from Hooke's law in Eq. (4) the stress and elastic strain increments in 5D are related by $d\vec{e}_{el}' = d\vec{s}'/2G$. A plastic

Table 3
Characteristics of the various NLK surface translation direction equations regarding number of parameters to be calibrated (NPC) for M surfaces (assuming the Δr_i and p_i from each yield surface are already identified) and ability to accurately model all uniaxial ratcheting conditions including rate decay (UR), or all multiaxial ratcheting conditions with constant rate (MRC) or with rate decay (MRD), to calibrate arbitrary uniaxial (U) or multiaxial ratcheting rates (M), and to independently calibrate arbitrary uniaxial and multiaxial ratcheting rates (UM).

Year	Kinematic model	NPC	UR	MRC	MRD	U	M	UM
1949	Prager [18]	0						
1966	Armstrong–Frederick [12]	M		✔		✔	✔	
1967	Mróz [6]	0		✔				
1979	Chaboche [13]	0		✔				
1986	Burlet–Cailletaud [20]	M			✔	✔	✔	
1993	Ohno–Wang I [21–22]	0			✔			
1993	Ohno–Wang II [21–22]	M	✔		✔	✔	✔	
1995	Delobelle [24]	$2M$		✔	✔	✔	✔	✔
1996	Jiang–Sehitoglu [17,23]	M	✔	✔	✔	✔	✔	
2004	Chen–Jiao [26]	$2M$	✔	✔	✔	✔	✔	✔
2004	Chen–Jiao (refined) [26]	$3M+1$	✔	✔	✔	✔	✔	✔
2005	Chen–Jiao–Kim [25]	$2M$	✔	✔	✔	✔	✔	✔

straining process beyond the yield surface would make it translate according to Eq. (6), preventing the stress state from crossing outside its boundary. The mathematical condition that guarantees that the new stress state $\vec{s}' + d\vec{s}'$ during a plastic process will remain on the yield surface border, without crossing outside it, is called consistency condition. Such infinitesimal condition can be calculated in the proposed E_{5s} space forcing the yield surface equation $Y = (\vec{s}' - \vec{\beta}')^T \cdot (\vec{s}' - \vec{\beta}') - S^2 = 0$ to remain valid throughout the surface translation process, thus

$$dY = 2 \cdot d\vec{s}'^T \cdot (\vec{s}' - \vec{\beta}') - 2 \cdot d\vec{\beta}'^T \cdot (\vec{s}' - \vec{\beta}') - 2 \cdot S \cdot dS = 0 \quad (17)$$

and, since the normal unit vector is such that $\vec{n}' = (\vec{s}' - \vec{\beta}')/|\vec{s}' - \vec{\beta}'| = (\vec{s}' - \vec{\beta}')/S$, then

$$d\vec{s}'^T \cdot \vec{n}' = d\vec{\beta}'^T \cdot \vec{n}' + dS \quad \text{(5D consistency condition)} \quad (18)$$

The scalar dS term in the consistency condition accounts for the variation of the yield surface radius S, gradually changing from the monotonic $S = S_Y$ to the cyclic $S = S_{Yc}$ in isotropic hardening and, in non-proportional (NP) loadings, to an NP-hardened yield strength $S = S_{YNP}$.

In the proposed incremental plasticity formulation, without loss of generality, instead of varying the radii $r_1 = S$ of the yield and r_i of the hardening surfaces (and consequently the radius differences $\Delta r_i \equiv r_{i+1} - r_i$), they are assumed constant, while isotropic and NP hardening effects are accounted for by changing the generalized plastic modulus coefficients p_i (instead of the Δr_i). Therefore, in this formulation where the yield surface radius $r_1 = S$ is assumed constant and thus $dS = 0$, the 5D consistency condition from Eq. (18) simplifies to $d\vec{s}'^T \cdot \vec{n}' = d\vec{\beta}'^T \cdot \vec{n}'$. Since the backstress increment $d\vec{\beta}'$ consists of the sum of the various backstress component increments $d\vec{\beta}' = d\vec{\beta}'_1 + d\vec{\beta}'_2 + \cdots + d\vec{\beta}'_M$, where each one has been defined in Eq. (6) as $d\vec{\beta}'_i = p_i \cdot \vec{v}'_i \cdot dp$, it follows that the consistency condition $d\vec{s}'^T \cdot \vec{n}' = d\vec{\beta}'^T \cdot \vec{n}'$ gives

$$d\vec{s}'^T \cdot \vec{n}' = d\vec{\beta}'^T \cdot \vec{n}' = (p_1 \cdot \vec{v}'^T_1 \cdot \vec{n}' + p_2 \cdot \vec{v}'^T_2 \cdot \vec{n}' + \cdots + p_M \cdot \vec{v}'^T_M \cdot \vec{n}') \cdot dp \quad (19)$$

In this formulation with surface radii r_i assumed constant, the values of p_i are initially calibrated to each surface using e.g. the monotonic stress–strain curve, and then corrected at every load cycle assuming they are directly proportional to the isotropic or NP hardening factors. For instance, after uniaxial isotropic hardening stabilization, every p_i would be multiplied by the S_{Yc}/S_Y ratio between the cyclic and monotonic yield strengths. In this way, it would be possible to assume constant yield and hardening surface radii without altering the stress–strain predictions.

The plastic flow rule in the proposed 5D deviatoric representation gives

$$d\vec{e}'_{pl} = \frac{1}{P} \cdot (d\vec{s}'^T \cdot \vec{n}') \cdot \vec{n}' \Rightarrow d\vec{s}'^T \cdot \vec{n}' = P \cdot \underbrace{d\vec{e}'^T_{pl} \cdot \vec{n}'}_{(3/2) \cdot dp} \Rightarrow P = \frac{2}{3} \cdot \frac{d\vec{s}'^T \cdot \vec{n}'}{dp}$$
$$(20)$$

Therefore, the generalized plastic modulus P needed to compute plastic straining can be expressed as a function of $\vec{v}'_i$ (as it would be expected for any "coupled formulation" [15]) through

$$P = (2/3) \cdot (p_1 \cdot \vec{v}'^T_1 + p_2 \cdot \vec{v}'^T_2 + \cdots + p_M \cdot \vec{v}'^T_M) \cdot \vec{n}' \quad (21)$$

The projections $\vec{v}'^T_i \cdot \vec{n}'$ of the generalized surface translation directions from Eq. (7) are given by

$$\vec{v}'^T_i \cdot \vec{n}' = \Delta r_i - \chi^*_i \cdot m^*_i \cdot \gamma_i \cdot [\delta_i + (1 - \delta_i)] \cdot \vec{\beta}'^T_i \cdot \vec{n}'$$
$$= \Delta r_i - \chi^*_i \cdot m^*_i \cdot \gamma_i \cdot \vec{\beta}'^T_i \cdot \vec{n}' \quad (22)$$

which, when combined to Eq. (21), allow the calculation of the associated generalized plastic modulus

$$P = (2/3) \cdot \sum_{i=1}^{M} p_i \cdot \left(\Delta r_i - \chi^*_i \cdot m^*_i \cdot \gamma_i \cdot \vec{\beta}'^T_i \cdot \vec{n}' \right) \quad (23)$$

For a given 5D stress increment $d\vec{s}' = A \cdot d\vec{\sigma}$, such P could then be used in the 5D version of the Prandtl–Reuss flow rule in Eq. (5') to obtain the total strain increment

$$d\vec{e}' = d\vec{e}'_{el} + d\vec{e}'_{pl} = \frac{d\vec{s}'}{2G} + \frac{1}{P} (d\vec{s}'^T \cdot \vec{n}') \cdot \vec{n}' \quad (24)$$

On the other hand, for a given 5D total strain increment $d\vec{e}' = A \cdot d\vec{\varepsilon}$, the 5D inverse problem could be solved (after some algebraic manipulation) by

$$d\vec{s}' = 2G \cdot d\vec{e}' - 2G \cdot \left[\frac{2G}{2G + P} d\vec{e}'^T \cdot \vec{n}' \right] \cdot \vec{n}' \quad (25)$$

After the entire stress or strain incremental integration in the computationally-efficient 5D spaces, the corresponding 6D values could be retrieved from the transformations described in Part I of this work:

$$\begin{cases} \vec{\sigma} = (2/3)A^T \cdot \vec{s}' + \vec{\sigma}_h \\ \vec{\varepsilon} = (2/3)A^T \cdot \vec{e}' + \vec{\varepsilon}_h \end{cases} \quad (26)$$

where the linear elastic hydrostatic components (assuming pressure-insensitive materials such as most metals) are easily calculated from the elastic relation $\vec{\sigma}_h = 3K \cdot \vec{\varepsilon}_h$, where $K = E/[3 \cdot (1 - 2v)]$ is the bulk modulus of the material.

5. Isotropic and NP hardening formulation in 5D

Isotropic and non-proportional (NP) hardening transients could also be incorporated into the proposed 5D formulation, through the varying values of the generalized plastic modulus coefficients p_i from each yield and hardening surface. From the Voce isotropic law and Tanaka's NP hardening equations [5], the values of p_i could be calculated as a function of the accumulated plastic strain $p \equiv \int dp$ from

$$p_i(p) = \underbrace{p_{ci} \cdot [1 + \alpha_{NP} \cdot F_{NP}(p)]}_{\text{NP evolution}} + \underbrace{(p_{mi} - p_{ci}) \cdot e^{-hr_c \cdot p}}_{\text{isotropic evolution}} \quad (27)$$

where p_{mi} and p_{ci} are the p_i coefficients calibrated respectively under uniaxial monotonic and cyclic conditions, hr_c is the material-dependent isotropic hardening rate, α_{NP} is the material-dependent additional hardening coefficient (with $0 \leqslant \alpha_{NP} \leqslant 1$), and $F_{NP}(p)$ is the load-path-dependent non-proportionality factor (with $0 \leqslant F_{NP}(p) \leqslant 1$).

The $F_{NP}(p)$ values are obtained in Tanaka's model [5] from a 5×5 polarization tensor $[P_T]$, whose evolution is given by

$$[dP_T] = (\vec{n}' \cdot \vec{n}'^T - [P_T]) \cdot hr_T \cdot dp \quad (28)$$

where hr_T is the material-dependent polarization rate and $\vec{n}'$ is the unit plastic straining direction in the proposed E_{5p} plastic strain space. From Tanaka's original model, it can be shown that the evolution equation of $F_{NP}(p)$ is given by

$$dF_{NP}(p) = \left[\sqrt{2 - \frac{2 \cdot |[P_T] \cdot \vec{n}'|^2}{tr\left([P_T]^T \cdot [P_T]\right)}} - F_{NP}(p) \right] \cdot hr_{NP} \cdot dp \quad (29)$$

where $tr(.)$ is the trace function, and hr_{NP} is the material-dependent NP hardening rate. Note that histories under free-surface conditions could adopt 3D or 2D sub-spaces of the defined 5D spaces, where

Tanaka's tensor would be represented respectively as 3×3 or 2×2 matrices, greatly reducing computational cost while evaluating Eq. (28) at every cycle. This is another major advantage of the 5D incremental plasticity formulation proposed in this work.

6. Notch formulation in 5D

The presented 5D spaces could also consider notch effects, without having to deal with 6D or tensor formulations. Two major 5D notch approaches could be followed: Pseudo-Material and Incremental Neuber/Molski–Glinka. Their application to the 5D formulation is discussed next.

6.1. Pseudo-material approach in 5D

For a given nominal stress history, the Pseudo-Material approach [27] could be used in 5D through the calibration of the generalized plastic modulus coefficients p_i to a fictitious material (a pseudo-material) with stress–strain behavior given by a nominal stress × notch strain curve, calculated under uniaxial conditions from a strain concentration rule such as Neuber or Molski–Glinka [28]. The 5D incremental plasticity formulation calibrated to this pseudo-material would then be used to calculate the notch-root strain history from the given multiaxial nominal stresses. After the entire notch strain history is obtained, the 5D incremental plasticity formulation is applied once more, but calibrated to the actual material properties (not the pseudo-material properties) to find the multiaxial notch stresses from the previously calculated multiaxial notch strains.

Conversely, for a given nominal strain history, a pseudo-material would be calibrated with stress–strain behavior given by a notch stress × nominal strain curve, calculated from a uniaxial model such as Neuber or Molski–Glinka. The notch-root stresses would then be calculated in the 5D formulation from the given nominal strains using the pseudo-material properties. The notch stress history is then input to a 5D incremental algorithm calibrated to the actual material properties, to find the corresponding multiaxial notch strains.

6.2. Incremental Neuber or Molski–Glinka

The original Neuber rule was derived for prismatic bodies loaded in pure shear, stating an equivalence between distortional strain energy densities, without including dilatational energies (which are zero under pure shear). Since Neuber's original relation did not include the dilatational strain energy density, Neuber's rule should assume that the total *distortional* strain energy density is constant for the pseudo and notch stress–strain curves [29]. Therefore, Neuber's incremental rule [30] adopts an equivalence of deviatoric stress and strain products, eliminating the influence of the hydrostatic components. Using the 6D-to-5D transformations defined in Part I of this work, it can be shown that Neuber's incremental rule can be represented in the proposed 5D formulation simply from

$$s_i \cdot de_i + e_i \cdot ds_i = \tilde{s}_i \cdot d\tilde{e}_i + \tilde{e}_i \cdot d\tilde{s}_i \quad \text{(5D Incremental Neuber)} \quad (30)$$

for $i = 1, 2, \ldots, 5$, where $\tilde{s}_i$ and $\tilde{e}_i$ are pseudo-values calculated (e.g. in a Finite Element program) assuming linear-elastic conditions, and s_i and e_i are the associated elastoplastic notch-root values. Molski–Glinka's rule [28] could also be used in an incremental deviatoric way in the proposed 5D formulation resulting, for $i = 1, 2, \ldots, 5$, in

$$s_i \cdot de_i = \tilde{s}_i \cdot d\tilde{e}_i \quad \text{(5D Incremental Molski} - \text{Glinka)} \quad (31)$$

One inconvenience of this approach (either in the original 6D or in the proposed 5D versions) is that it requires the solution of a set of equations such as the ones from Eq. (30) or (31), which can be computationally costly in an implicit integration formulation.

Finally, a Modified Boundary Condition approach [31] could also be followed, easily adaptable to the proposed 5D formulation since a single strain energy equation is required, with the remaining equations coming from assumptions on the ratios of pseudo and notch components.

7. Experimental validation

The proposed 5D incremental plasticity formulation has been implemented in the ViDa 3D software [32] to predict multiaxial elastoplastic stress–strain relations. Isotropic, non-proportional (NP), and all presented non-linear kinematic hardening models were simulated in the 5D formulation for various representative loading paths. The numerical robustness of the algorithm was verified using the same model in both stress and strain control, as recommended in [33], i.e. the stress history is calculated in the code from a given strain history, and then the computed stresses are used as input to the same code to predict the original strain history, with negligible errors of the order of the computation resolution. A large number of conducted simulations using unbalanced load histories confirmed all conclusions summarized in Table 3 about the characteristics of different kinematic hardening models.

For the experimental verification, simulations were performed using the proposed generalized surface translation rule from Eqs. (7) and (8), calibrated to describe Jiang–Sehitoglu's model. To improve the calculation accuracy, the backstress was divided into 10 additive components, following Chaboche's idea [13], with stress increments at each integration step limited to only 2 MPa. Jiang–Sehitoglu's material parameters were calibrated from uniaxial data using the procedure described in [23].

Tension–torsion experiments were performed on tubular annealed 316L stainless steel specimens in an MTS 809.25 testing machine, see Fig. 5. The cyclic properties of this steel were obtained from uniaxial tests. Engineering stresses and strains were measured using a load/torque cell and the MTS 632.68 axial/torsional extensometer.

One of the experimented strain-controlled tension–torsion tests adopted strain paths describing a square pulse in the $\varepsilon_x \times \gamma_{xy}/\sqrt{3}$ strain diagram, see Fig. 6. The predicted and measured stress paths after isotropic and NP hardening stabilization show good
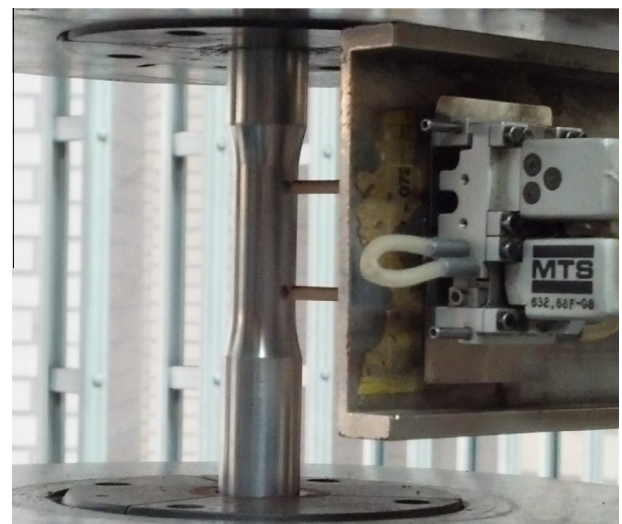
Fig. 5. Tubular specimen mounted in an MTS tension–torsion machine, showing the axial/torsional extensometer.
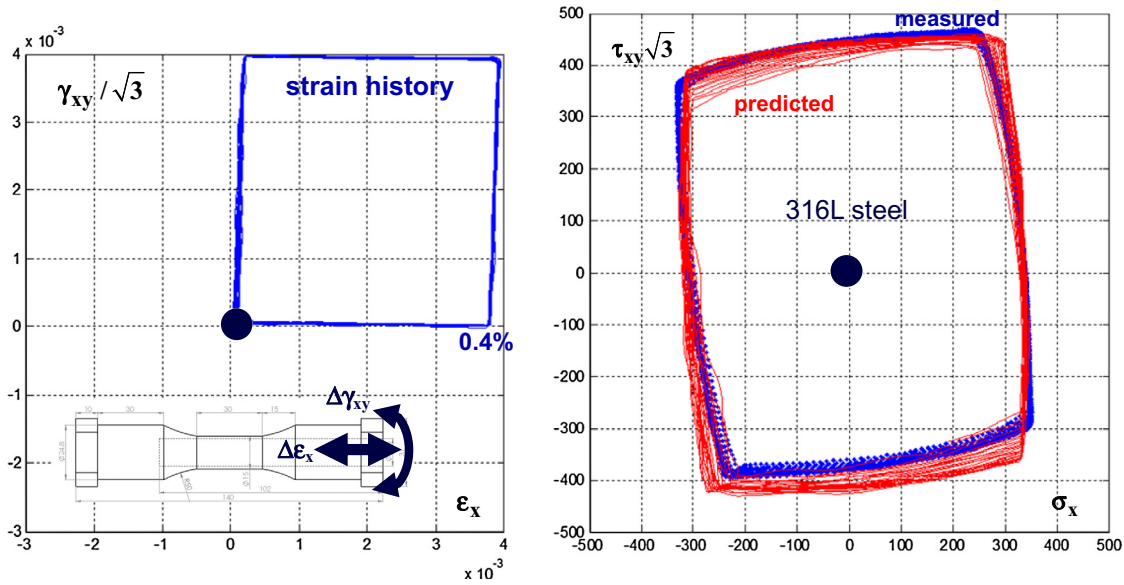
Fig. 6. Stress path predictions from the proposed formulation for a strain-controlled square pulse on a tension–torsion 316L steel tubular specimen, showing a good experimental agreement in the presence of significant mean stress relaxation.

agreement even in the presence of significant mean stress relaxation, as it can be observed from the low resulting mean stresses in the almost symmetrical stress paths, despite the high applied mean strains. The same calibrated parameters from the proposed generalized surface translation rule were later used to predict multiaxial ratcheting under stress control, also showing a very good experimental agreement. These results confirm that ratcheting and mean stress relaxation are indeed two aspects of the same phenomenon, which become evident respectively under stress and strain control.

To evaluate the ability of the proposed formulation to predict as well uniaxial ratcheting, uniaxial tension–compression experiments were performed on cylindrical specimens made of 1020 steel with yield strength 365 MPa and ultimate strength 542 MPa. An unbalanced history between −200 and 350 MPa was imposed under stress control, with a mean stress component that induced uniaxial ratcheting, see Fig. 7. As shown in the figure, by adopting a calibration that describes Jiang–Sehitoglu's kinematic hardening model, the proposed formulation is able to predict the

ratcheting rate decay observed in the first 100 cycles of such unbalanced loading.

Note that all tension–torsion simulations were performed in 2D sub-spaces of the proposed 5D stress and strain spaces, significantly decreasing computational cost, especially since both isotropic and NP hardening transients were considered. The simulations were repeated adopting a traditional 6D incremental plasticity formulation, resulting in the exact same path predictions but with a computational time about 100% higher than the one spent using the proposed formulation. Therefore, the proposed 5D framework is recommended due to its significantly lower computational cost, without any loss in calculation accuracy while considering isotropic and NP hardening transients, non-linear kinematic hardening, and notch effects.

8. Conclusions

In this work, an incremental plasticity formulation was proposed, entirely represented in efficient reduced-order five-dimensional (5D) stress and strain spaces. A generalized surface translation equation was proposed in 5D, from which all main non-linear kinematic (NLK) hardening models are a special case. The proposed 5D formulation can be easily transformed into 3D, 2D, or 1D representations of stresses and strains, to most efficiently calculate the stress–strain behavior under free-surface, tension–torsion, or uniaxial conditions, respectively. Such representations in lower dimensions could reduce in more than half the computational cost of incremental plasticity calculations, without altering the resulting predictions. Experiments with 316L and 1020 steel specimens confirmed the efficiency of the proposed framework to compute ratcheting and mean stress relaxation, which can have important effects on fatigue lives due to premature exhaustion of the material ductility and to changes in mean and maximum stresses.

Acknowledgments
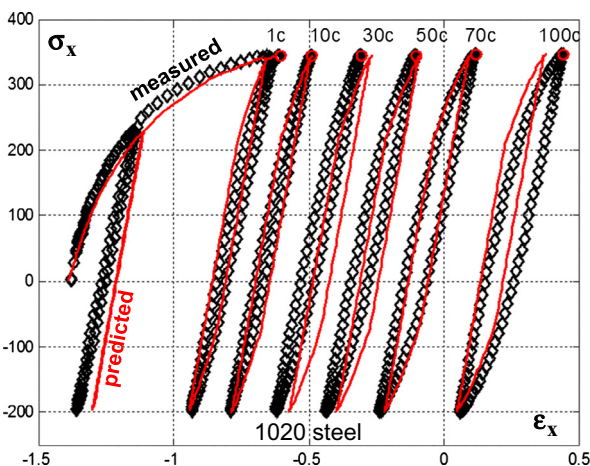
Fig. 7. Uniaxial ratcheting predictions from the proposed formulation for a 1020 steel cylindrical specimen, showing the predicted and measured uniaxial loops after 1, 10, 30, 50, 70 and 100 cycles.

References

[1] Ilyushin AA. On the foundations of the general mathematical theory of plasticity. In: Voprosy Teorii Plastichnosti, Moskva: Izd. AN SSSR; 1961. p. 3–29 [in Russian].

[2] Meggiolaro MA, Castro JTP. An improved multiaxial rainflow algorithm for non-proportional stress or strain histories – Part I: Enclosing surface methods. Int J Fatigue 2012;42:217–26.

[3] Meggiolaro MA, Castro JTP. Prediction of non-proportionality factors of multiaxial histories using the moment of inertia method. Int J Fatigue 2014;61:151–9.

[4] Meggiolaro MA, Castro JTP. An improved multiaxial rainflow algorithm for non-proportional stress or strain histories – Part II: The modified Wang–Brown method. Int J Fatigue 2012;42:194–206.

[5] Tanaka E. A nonproportionality parameter and a cyclic viscoplastic constitutive model taking into account amplitude dependences and memory effects of isotropic hardening. Eur J Mech A Solids 1994;13:155–73.

[6] Mróz Z. On the description of anisotropic workhardening. J Mech Phys Solids 1967;15(3):163–75.

[7] Garud YS. A new approach to the evaluation of fatigue under multiaxial loading. Trans ASME J Eng Mater Technol 1981;103:118–25.

[8] Krieg RD. A practical two-surface plasticity theory. J Appl Mech 1975;42 (3):641–6.

[9] Dafalias YF, Popov EP. Plastic internal variables formalism of cyclic plasticity. J Appl Mech 1976;43(4):645–51.

[10] Chaboche JL. A review of some plasticity and viscoplasticity constitutive theories. Int J Plast 2008;24(10):1642–93.

[11] Jiang Y, Sehitoglu H. Comments on the Mróz multiple surface type plasticity models. Int J Solids Struct 1996;33(7):1053–68.

[12] Armstrong PJ, Frederick CO. A mathematical representation of the multiaxial Bauschinger effect. CEGB Report RD/B/N731, Berkeley Nuclear Laboratory; 1966.

[13] Chaboche JL, Dang Van K, Cordier G. Modelization of the strain memory effect on the cyclic hardening of 316 stainless steel. In: Transactions of the fifth international conference on structural mechanics in reactor technology, Div. L, Berlin; 1979.

[14] Ohno N, Wang JD. Transformation of a nonlinear kinematic hardening rule to a multisurface form under isothermal and nonisothermal conditions. Int J Plast 1991;7:879–91.

[15] Bari S, Hassan T. Kinematic hardening rules in uncoupled modeling for multiaxial ratcheting simulation. Int J Plast 2001;17(7):885–905.

[16] Jiang Y, Kurath P. Characteristics of the Armstrong–Frederick type plasticity models. Int J Plast 1996;12:387–415.

[17] Jiang Y, Sehitoglu H. Modeling of cyclic ratchetting plasticity, Part I: Development of constitutive relations. ASME J Appl Mech 1996;63(3):720–5.

[18] Prager W. Recent developments in the mathematical theory of plasticity. J Appl Phys 1949;20(3):235–41.

[19] Abdel Karim M, Ohno N. Kinematic hardening model suitable for ratcheting with steady-state. Int J Plast 2000;16:225–40.

[20] Burlet H, Cailletaud G. Numerical techniques for cyclic plasticity at variable temperature. Eng Comput 1986;3(2):143–53.

[21] Ohno N, Wang JD. Kinematic hardening rules with critical state of dynamic recovery, Part I: Formulations and basic features for ratchetting behavior. Int J Plast 1993;9:375–90.

[22] Ohno N, Wang JD. Kinematic hardening rules with critical state of dynamic recovery, Part II: Application to experiments of ratchetting behavior. Int J Plast 1993;9:391–403.

[23] Jiang Y, Sehitoglu H. Modeling of cyclic ratchetting plasticity, Part II: Comparison of model simulations with experiments. ASME J Appl Mech 1996;63(3):726–33.

[24] Delobelle P, Robinet P, Bocher L. Experimental study and phenomenological modelization of ratchet under uniaxial and biaxial loading on an austenitic stainless steel. Int J Plast 1995;11:295–330.

[25] Chen X, Jiao R, Kim KS. On the Ohno–Wang kinematic hardening rules for multiaxial ratcheting modeling of medium carbon steel. Int J Plast 2005;21:161–84.

[26] Chen X, Jiao R. Modified kinematic hardening rule for multiaxial ratcheting prediction. Int J Plast 2004;20:871–98.

[27] Barkey ME, Socie DF, Hsia KJ. A yield surface approach to the estimation of notch strain for proportional and nonproportional cyclic loading. J Eng Mater Technol 1994;116:173–80.

[28] Molski K, Glinka G. A method of elastoplastic and strain calculation at a notch root. Mater Sci Eng 1981;50:93–100.

[29] Kujawski D. On energy interpretations of the Neuber's rule. Theoret Appl Fract Mech 2014;73:91–6.

[30] Ince A, Glinka G. A numerical method for elasto-plastic notch-root stress–strain analysis. J Strain Anal Eng Des 2013;48(4):229. 229-224.

[31] McDonald RJ, Socie DF. A technique to estimate the local multiaxial elastic–plastic behavior from a purely elastic solution. Eng Fract Mech 2011;78:1696–704.

[32] Meggiolaro MA, Castro JTP. Automation of the fatigue design under variable amplitude loading using the ViDa software. Int J Struct Integrity 2010;1:1–6.

[33] Socie DF, Marquis GB. Multiaxial fatigue. SAE; 1999.